

University of Groningen

The Impact of Stoichiometry on the Photophysical Properties of Ruddlesden-Popper Perovskites

Duim, Herman; Adjokatse, Sampson; Kahmann, Simon; ten Brink, Gert H.; Loi, Maria Antonietta

Published in:
Advanced Functional Materials

DOI:
[10.1002/adfm.201907505](https://doi.org/10.1002/adfm.201907505)

IMPORTANT NOTE: You are advised to consult the publisher's version (publisher's PDF) if you wish to cite from it. Please check the document version below.

Document Version
Publisher's PDF, also known as Version of record

Publication date:
2019

[Link to publication in University of Groningen/UMCG research database](#)

Citation for published version (APA):

Duim, H., Adjokatse, S., Kahmann, S., ten Brink, G. H., & Loi, M. A. (2019). The Impact of Stoichiometry on the Photophysical Properties of Ruddlesden-Popper Perovskites. *Advanced Functional Materials*, Article 1907505. <https://doi.org/10.1002/adfm.201907505>

Copyright

Other than for strictly personal use, it is not permitted to download or to forward/distribute the text or part of it without the consent of the author(s) and/or copyright holder(s), unless the work is under an open content license (like Creative Commons).

The publication may also be distributed here under the terms of Article 25fa of the Dutch Copyright Act, indicated by the "Taverne" license. More information can be found on the University of Groningen website: <https://www.rug.nl/library/open-access/self-archiving-pure/taverne-amendment>.

Take-down policy

If you believe that this document breaches copyright please contact us providing details, and we will remove access to the work immediately and investigate your claim.

Downloaded from the University of Groningen/UMCG research database (Pure): <http://www.rug.nl/research/portal>. For technical reasons the number of authors shown on this cover page is limited to 10 maximum.

The Impact of Stoichiometry on the Photophysical Properties of Ruddlesden–Popper Perovskites

Herman Duim, Sampson Adjokatse, Simon Kahmann, Gert H. ten Brink, and Maria Antonietta Loi*

2D Ruddlesden–Popper perovskites are interesting for a variety of applications owing to their tunable optical properties and their excellent ambient stability. As these materials are processable from solution, they hold the promise of procuring flexible and cost-effective films through large-scale fabrication techniques. However, such solution-based deposition techniques often induce large degrees of heterogeneity due to poorly controlled crystallization. The microscopic properties of films of (PEA)₂PbI₄ cast from precursor solutions of different stoichiometry are therefore investigated. The stoichiometry of the precursor solution is found to have a large impact on the crystallinity, morphology, and optical properties of the resulting thin films. Even for films cast from stoichiometric precursors, differences in photoluminescence intensities occur on a subgranular level. The heterogeneity in these films is found to be thermally activated with an activation energy of 0.4 eV for the emergence of local variations in nonradiative recombination rates. The spatial variation in the distribution of trap states is attributed to local fluctuations in the stoichiometry. In line with this, the surface can successfully be passivated by providing an excess of phenylethylammonium iodide (PEAI) to an as-cast film, enhancing the photoluminescence by as much as 85% without significantly altering the film's morphology.

tunable band gap, and long charge carrier diffusion lengths^[1,2] make these materials exceedingly good materials for photovoltaics, with power conversion efficiencies now reaching values as high as 25.2%.^[3] The recent string of successes of metal halide perovskites is, however, by no means limited to photovoltaics, but extends to a myriad of other optoelectronic applications such as light-emitting diodes, photonic devices, X-ray detectors, and gas sensors.^[4–10]

The closely related perovskite-like compounds of lower dimensionality (2D, 1D, and 0D) have also attracted considerable attention in recent years owing to their versatile photophysical properties and suitability for light emission.^[11] Of these low-dimensional perovskites, the most widely studied are the Ruddlesden–Popper (RP) perovskite phases of the form A'₂A_{n-1}BnX_{3n+1}. In these (quasi-) 2D perovskites, thin sheets of perovskite of layer thickness *n* are sandwiched between long organic cations A', leading to the natural

formation of multiple-quantum-well structures.^[12,13] The strong quantum and dielectric confinement of charge carriers in these perovskite layers give rise to exciton binding energies that can be as large as a few hundred meV, depending on the thickness of the perovskite layer.^[14,15] By tuning the length and nature of the spacer cation or the thickness and composition of the perovskite layer, emitted light can be tuned from the violet to the near-infrared spectral region.^[16] Using this approach, bright blue,^[17] green,^[17,18] and red^[19] light-emitting diodes with high color-purity have already been successfully reported.^[20]


Recently, we have demonstrated that high-quality pinhole-free films of the 2D perovskite 2-phenylethylammonium lead iodide ((PEA)₂PbI₄) can be fabricated using a scalable blade-coating technique.^[21] Not only does this pave the way for the fabrication of large-area devices based on 2D perovskites, but these films can also be used as excellent templates for the formation of high-quality 3D perovskite films through a cation exchange reaction.^[21–23] As such, blade-coated films of 2D perovskite hold great potential for fabrication of large-area perovskite layers for a wide variety of optoelectronic applications. Typically, however, metal halide perovskites suffer from a large degree of heterogeneity in properties such as grain sizes, crystallinity, trap state densities and chemical composition in the resulting thin films owing to poor control over the crystallization.^[24] Such structural disorder arising from the fabrication conditions can have a significant impact on the material's optoelectronic properties.^[25]

1. Introduction

Metal halide perovskite semiconductors of the form ABX₃, where A is a monovalent cation, B a divalent metal cation, and X a halide anion, have shown great promise for the development of versatile and high-efficiency optoelectronic devices owing to their outstanding photophysical properties. Their strong light absorption,

H. Duim, Dr. S. Adjokatse, Dr. S. Kahmann, Prof. M. A. Loi
Photophysics and OptoElectronics
Zernike Institute for Advanced Materials
University of Groningen
Nijenborgh 4, 9747 AG Groningen, The Netherlands
E-mail: m.a.loi@rug.nl

G. H. ten Brink
Nanostructured Materials and Interfaces
Zernike Institute for Advanced Materials
University of Groningen
Nijenborgh 4, 9747 AG Groningen, The Netherlands

 The ORCID identification number(s) for the author(s) of this article can be found under <https://doi.org/10.1002/adfm.201907505>.

© 2019 The Authors. Published by WILEY-VCH Verlag GmbH & Co. KGaA, Weinheim. This is an open access article under the terms of the Creative Commons Attribution-NonCommercial-NoDerivs License, which permits use and distribution in any medium, provided the original work is properly cited, the use is non-commercial and no modifications or adaptations are made.

DOI: 10.1002/adfm.201907505

In this work, we, therefore, investigate the (microscopic) photoluminescence (PL) properties of blade-coated films of the archetypal pure 2D RP perovskite ((PEA)₂PbI₄) in relation to the stoichiometry of their precursor solution. We obtain macroscopically smooth and uniform films of the RP perovskite for different stoichiometries, but by using confocal laser scanning microscopy (CLSM), we show that the photoluminescence properties are highly heterogeneous on a microscopic scale. The PL intensity is locally enhanced even within individual grains at the perovskite–air interface, which we attribute to variations in the density of defect states owing to fluctuations of the stoichiometry in the precursor solution during crystallization. The extent of the heterogeneity in thin films on a microscopic scale is an important consideration for their implementation in devices and can easily be overlooked given that these variations occur on a scale smaller than the typical laser spot sizes used in conventional PL measurements.

2. Results and Discussion

2.1. Passivation of Surface Trap States

A scalable blade-coating technique was used to deposit thin films of the Ruddlesden–Popper perovskite (PEA)₂PbI₄, of

which a schematic crystal structure is provided in **Figure 1a**. The high quality of the films fabricated via this method is evidenced by the complete surface coverage and a high degree of orientation and narrow linewidths in the XRD pattern, as reported in Figure S1 (Supporting Information).^[26] Optically, these films exhibit typical narrow exciton absorption and emission lines with a small Stokes shift of 17 nm (Figure S1, Supporting Information). The photoluminescence has an FWHM linewidth of only 18 nm with CIE-color coordinates $x = 0.191$, $y = 0.783$, and a corresponding color purity of 94.9%. The photoluminescence quantum yield (PLQY) of the blade-coated film was measured to be 1.4%, which is substantially higher than previously reported PLQY values for thin films of (PEA)₂PbI₄ (<0.1%)^[27] and (PEA)₂PbBr₄ (0.35%).^[28] CLSM reveals the presence of large spatial heterogeneities in PL intensities in these films, as shown in Figure 1b, indicating large differences in local trap state densities. A similar observation can also be made for films that are spin cast albeit on a smaller scale (Figure S2, Supporting Information).

In a previous work, we have established the important role the surface chemistry plays in the passivation of surface trap states of the 3D perovskite CH₃NH₃PbBr₃.^[29] In line with this and recent reports on the successful passivation of trap states in both 3D and 2D perovskites,^[18,30,31] we attempt to remedy any surface trap states introduced by vacancies such

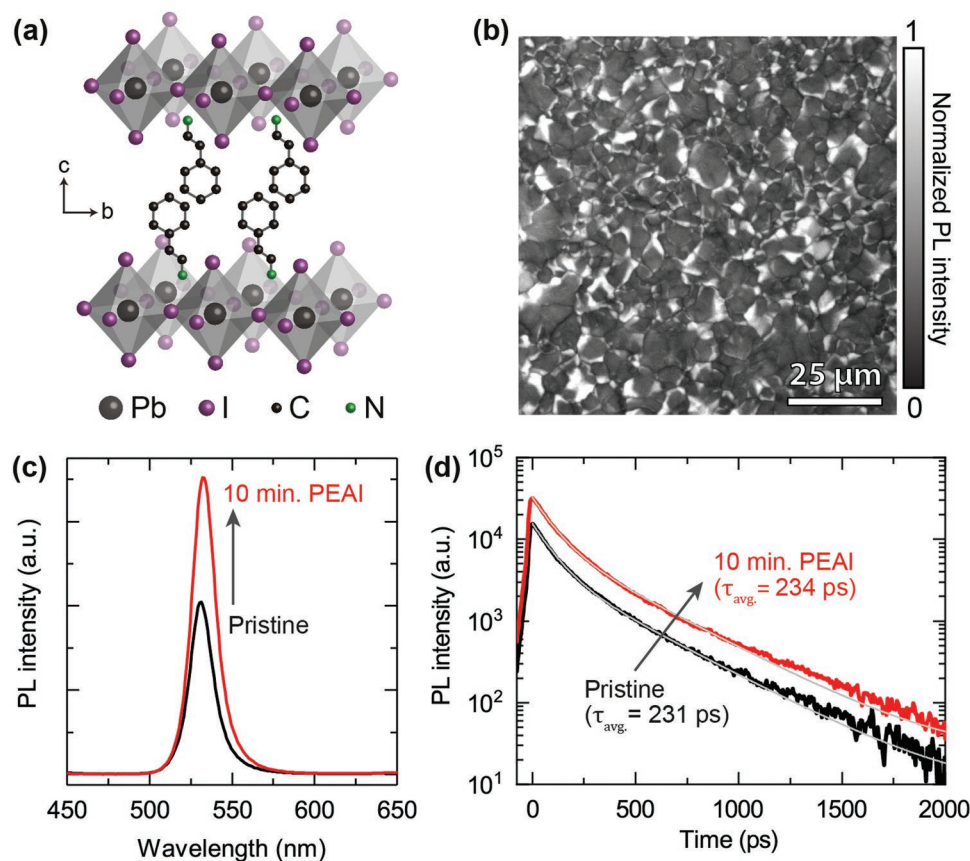


Figure 1. a) Schematic representation of the crystal structure of (PEA)₂PbI₄. b) Normalized PL intensity map of a blade-coated film of (PEA)₂PbI₄. c) Steady-state PL spectra of the film before and after surface treatment and d) the corresponding TRPL decays, fitted by biexponential decays with lifetimes $\tau_{\text{fast}} = 91$ ps, $\tau_{\text{slow}} = 330$ ps and relative weight factors of $A_{\text{fast}} = 72\%$ (71%) and $A_{\text{slow}} = 28\%$ (29%) for the pristine (10 min, PEAI) film.

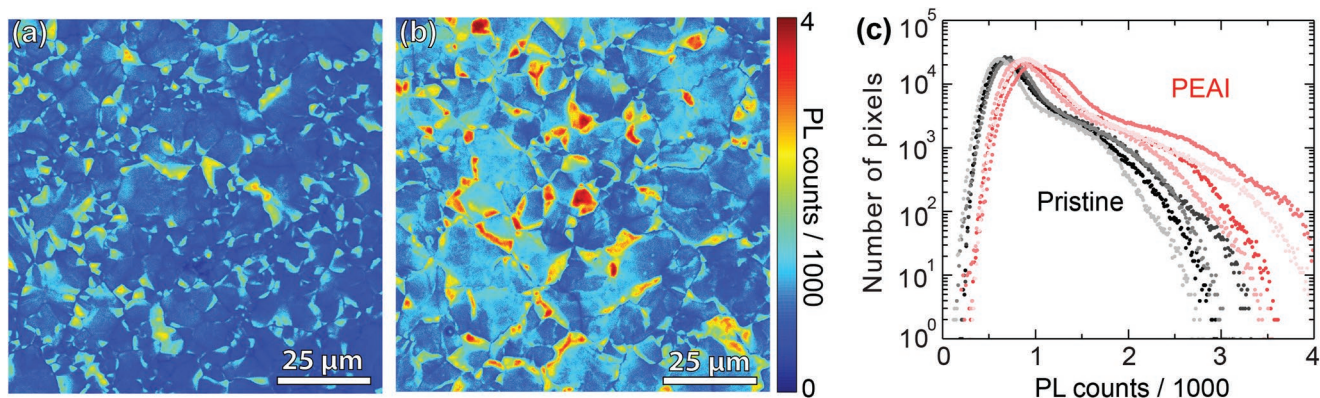


Figure 2. CLSM photoluminescence intensity maps of a) a pristine film of (PEA)₂PbI₄ and b) the same film after 10 min of PEAI treatment. Both images are displayed on the same intensity scale for comparison. c) Histograms obtained from four 100 × 100 μm² areas of the same film before (black) and after (red) PEAI treatment.

as V_{PEA} , V_{I} , and V_{PEAI} that might result from PEAI-poor conditions during the film's crystallization. We purposely passivate the surface of an as-cast film through a simple ligand treatment. After submerging the films in a solution of PEAI in isopropanol (IPA) (50×10^{-3} M) for 10 min, an increase in the average photoluminescence intensity by 85% was observed, as is shown in Figure 1c. If the ligand treatment is too short (30 s), however, no PL increase is observed. Furthermore, if the film is exposed to IPA alone, the film partially dissolves and the PL is quenched (Figure S3, Supporting Information). These findings consolidate our prior assumption that PEAI plays an important role in the surface chemistry of the (PEA)₂PbI₄ film.

Paradoxically, from the time-resolved PL (TRPL) data in Figure 1d, it becomes clear that the average exciton lifetimes are not significantly affected by the ligand treatment as would typically be expected for the elimination of slow trapping processes. The increase in the integrated PL intensity instead stems from an increased PL intensity at $t = 0$ (normalized TRPL as well as data for shorter delay times are provided in Figure S4 in the Supporting Information). Assuming that the absorption of the film does not significantly change with the ligand treatment, this means that the exciton population participating in radiative recombination must have increased after the ligand treatment. This suggests that initially a sizable number of excitons undergo ultrafast nonradiative recombination on a time scale shorter than the temporal resolution of our detector (<2 ps). The ligand treatment seems to effectively suppress this recombination channel, presumably through the removal of vacancies of PEA, PEAI or iodide.

To further investigate the effect of PEAI on the perovskite surface, we performed CLSM on a film before and after the ligand treatment. Figure 2a,b shows a side-by-side comparison of the PL intensity map of the pristine film and the film after PEAI treatment. In both cases, a large degree of spatial heterogeneity in PL intensity can be observed. Upon passivation, a clear overall increase in PL intensity is readily observed from these images. The semilogarithmic histograms representing the distribution of the pixels' PL counts of the maps in Figure 2c show the presence of two superimposed pixel populations. Here, the main pixel distribution is relatively narrow

and is centered at PL counts just below 1000. Superimposed on this is a much broader population of pixels extending to high PL values that stems from the presence of the brightest areas in Figure 2a,b. Upon PEAI treatment, both these pixel populations show a shift to higher PL counts accompanied by a significant broadening. This corresponds to an overall increase in PL intensity which is visible as a brightening of both the darker as well as the brighter areas of the pristine film.

2.2. Influence of Stoichiometry on the Film Quality

We then investigated the influence of the stoichiometry of the precursor solution on the blade-coated film quality and optical properties. We cast (PEA)₂PbI₄ films according to a well-established recipe,^[32,33] i.e., precursor solutions in a mixture of solvents (DMF:DMSO 4:1 v/v) of different stoichiometry that are either lead-rich (molar ratio PEAI:PbI₂ = 1:2, 1:1), stoichiometric (2:1) or lead-poor (3:1 and 4:1).

The absolute intensities of the PL in Figure 3a show that the highest PL intensity is obtained when a stoichiometric precursor solution (PEAI:PbI₂ = 2:1) is employed. Films cast from a solution with a relative excess of PbI₂ exhibit a significant decrease in the PL intensity, whereas large excesses of PEAI only have a minimal effect on the photoluminescence intensity of the film. This is in line with a recent report from our group, in which we demonstrated the severe reduction in PL quantum yield upon photo-induced degradation of (PEA)₂PbI₄ to PbI₂ due to the loss of organic cations from the crystal surface.^[34] Interestingly, the presence of large amounts of PbI₂ also effectively suppresses the broad low-energy emission that is (weakly) present in the stoichiometric and PEAI-rich films (Figure S5, Supporting Information). Such broad emission bands are often observed in low-dimensional perovskite and their nature is the topic of ongoing debate. Often they are attributed to the recombination of self-trapped excitons.^[35] At this point, we merely mean to highlight that the strong dependence of this broad emission on the stoichiometry of the precursor solution suggests an extrinsic origin and we shall further confront this issue in a separate report.

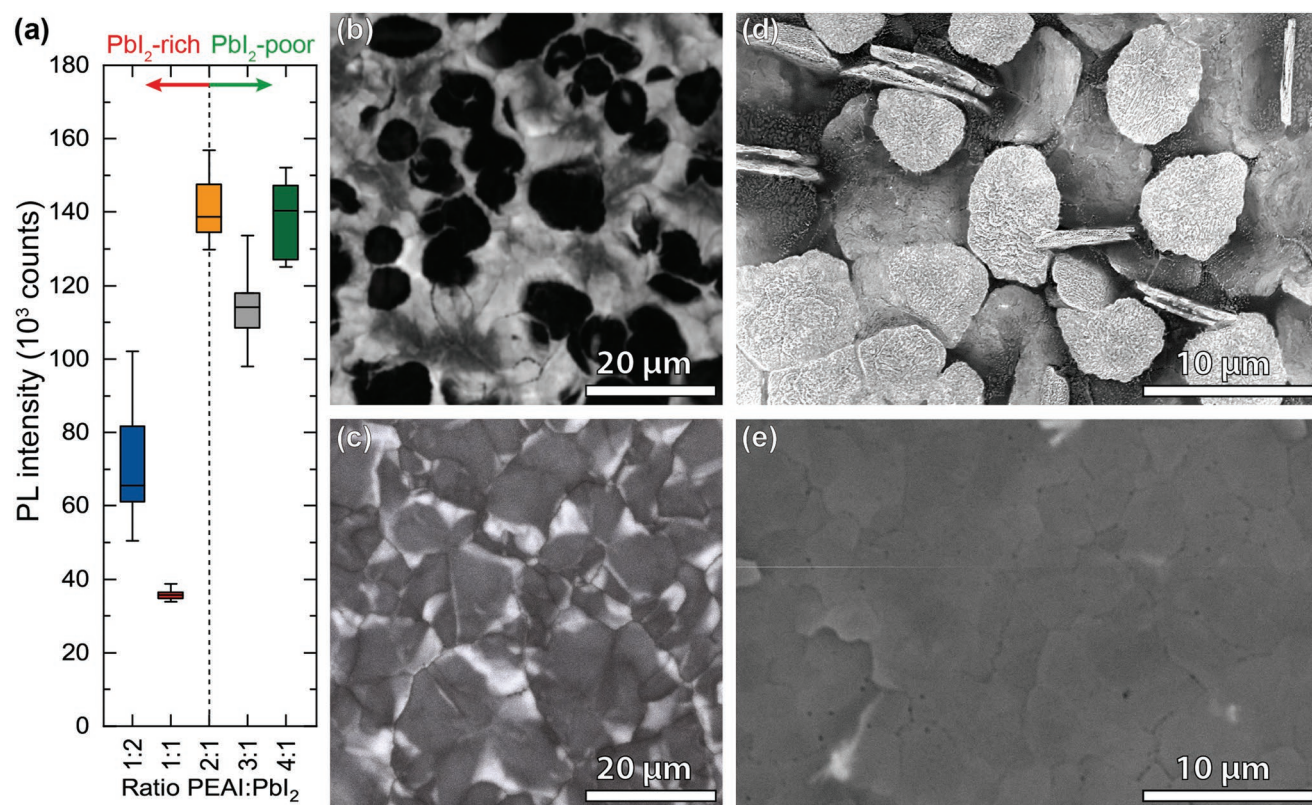


Figure 3. a) Boxplot of the PL intensities of films cast from precursor solutions of different stoichiometry showing a clear intensity reduction for lead-rich films. Individual boxplots are based on five data points per sample. b) CLSM PL map of the lead-rich (PEAl:PbI₂ = 1:2) and c) stoichiometric (2:1) film. d,e) SEM images obtained from the same films as in (b) and (c), respectively.

While all blade-coated films show complete surface coverage, moving away from stoichiometry to either an excess or deficit of PbI₂ has a pronounced impact on the film's morphology. This impact can be readily observed from the reflected light and CLSM images in Figure S6 (Supporting Information). Of particular interest are the stoichiometric (2:1) and the lead-rich case (PEAl:PbI₂ ratio of 1:2), on which we focus in Figure 3b–e. The spatially resolved PL map obtained from the lead-rich film (Figure 3b) shows the presence of large areas of quenched luminescence surrounded by a network of brightly emitting film. Contrarily, in the case of the stoichiometric film, the PL map in Figure 3c shows the presence of densely packed grains separated by darkened grain boundaries, as well as areas of increased PL intensity in the interior of apparent grains. Comparison of the features in these PL maps to the film's morphology, as observed by scanning electron microscopy (SEM) in Figure 3d,e shows that the quenched PL in the lead-rich film coincides with the presence of large platelets on the perovskite surface. We assign these platelets to be clusters of lead iodide, the formation of which is corroborated by prominent diffraction peaks from PbI₂ (Figure S7, Supporting Information). Additionally, the reduced intensity and broadening of the diffraction peaks from the (00*n*) perovskite planes indicates the considerably poorer crystallinity compared to that of the stoichiometric film, solidifying the notion that the presence of large quantities of PbI₂ has a negative impact on the crystallization in these doctor bladed films. The SEM

image of the stoichiometric film (Figure 3e), on the other hand, shows a flat and featureless surface topography with faintly visible grain boundaries, but no apparent correlation between the film's morphology and the local variations in PL intensity (Figure 3c). We shall discuss this issue further below.

For films blade-coated from solutions that lie closer to the ideal stoichiometry of 2:1 (namely, 2:1.3, 2:1.1, 2.1:1, and 2.3:1), the observed changes are less severe. A minor increase in PL intensity can be observed for films that are cast from a 2:1.3 solution, while all other stoichiometries result in a modest reduction of PL intensities, showing the lack of a real trend, as can be seen in Figure S8 (Supporting Information). The PL maps of these films reveal that going from the lead-rich condition of 2:1.3 to the PEA-rich conditions, the degree of heterogeneity increases considerably (Figure 4). Under slightly PbI₂-rich conditions, heterogeneity is suppressed to a large extent in the PL map of these films as compared to that of the stoichiometric film. Here, however, we should be careful as many different effects can contribute to this observation. A different starting stoichiometry can determine a very different nucleation mechanism and even a different film thickness. Certainly not comparable to what is obtained with the post-treatment with one of the precursors (vide supra). Interestingly, when exchanging phenylethylammonium for butylammonium (BA) the photoluminescence of the resulting films is strongly quenched, as can be seen from the full-color photographs of the (PEA)₂PbI₄ and (BA)₂PbI₄ films under UV excitation (Figure S9, Supporting Information). The

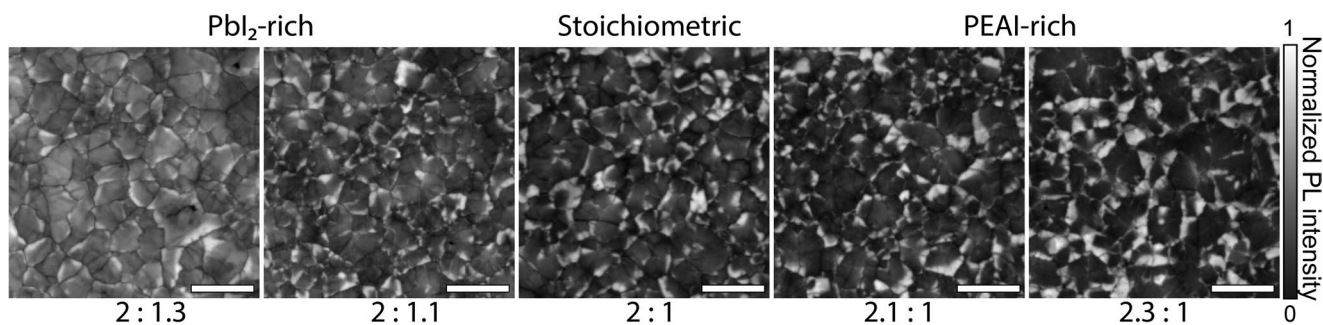


Figure 4. Normalized PL maps of films cast from precursor solutions with small deviations from stoichiometry, as indicated by the PEA1:PbI₂ ratios listed below the PL map of the corresponding film. Scale bars are 25 μm.

latter film is considerably rougher and its PL map (Figure S10, Supporting Information) reveals the presence of large grains with limited PL heterogeneity; demonstrating that also the nature of the organic cation plays an important role in the crystallization and distribution of trap states in 2D perovskites.

2.3. PL Heterogeneity in Blade-Coated Films

Clearly, large variations in PL intensity exist throughout the film on a microscopic level despite the excellent surface

coverage and homogeneity of all blade-coated films on a macroscopic scale, and are strongly dependent on the stoichiometry of the precursor solution. It is especially interesting that even in the case where a stoichiometric solution is used, considerable spatial fluctuations in PL intensities still persist.

The reflected laser light micrograph (800 nm) in Figure 5a shows the presence of distinct grain boundaries. The same large grain boundaries are also clearly observable as areas of low luminescence in the PL map in Figure 5b, as well as some smaller boundaries that are not observable through reflected

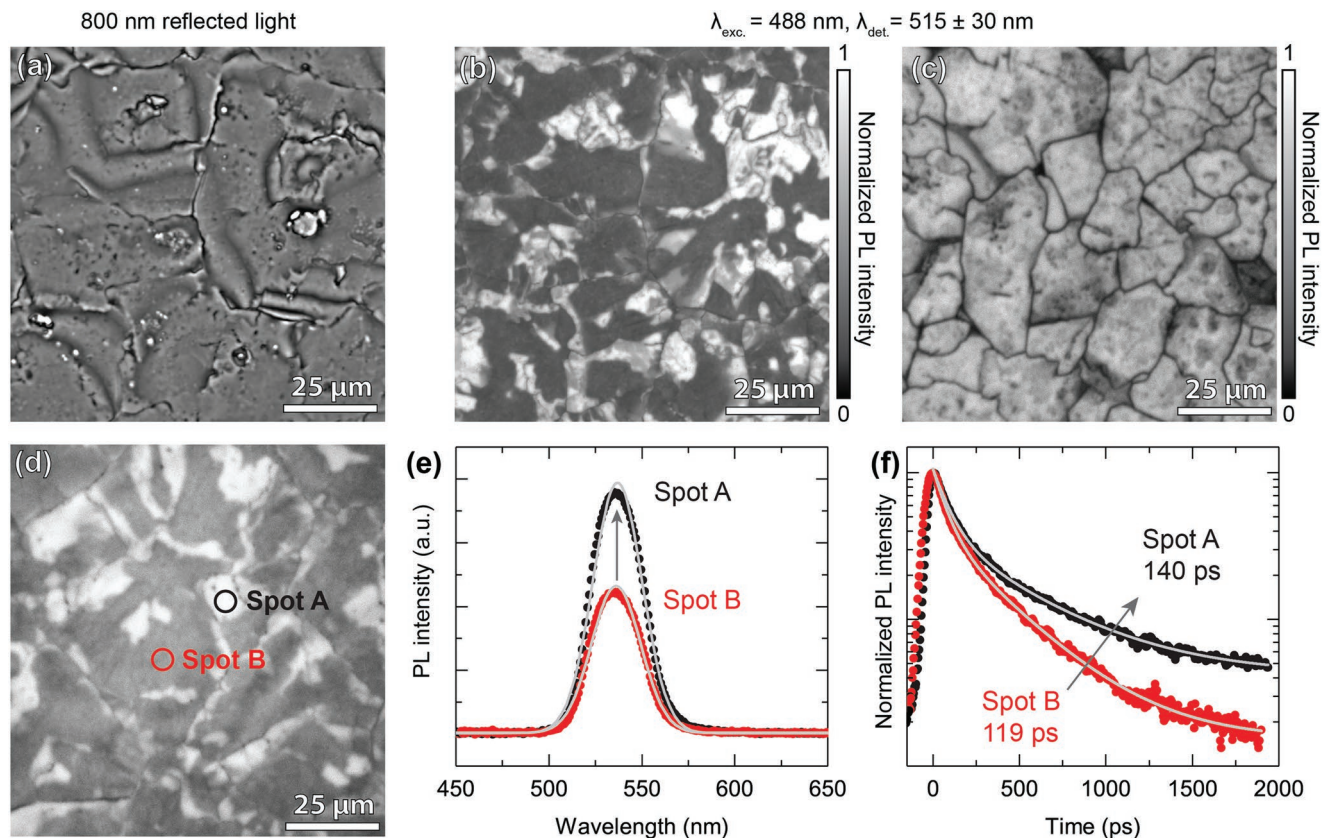


Figure 5. a) Reflected light micrograph obtained from a stoichiometric film using the reflection of an 800 nm laser, showing the surface morphology of the film. b) Normalized PL map obtained by exciting the (PEA)₂PbI₄ film at the perovskite–air interface and c) from the perovskite–glass interface with a 488 nm cw laser. d) Grayscale intensity map of the photoluminescence intensity of a blade-coated (PEA)₂PbI₄ film obtained using CLSM with a 400 nm pulsed laser. e) Steady-state photoluminescence spectra measured at the bright spot A (black) and the dark spot B (red) along with f) their corresponding PL decay traces. Solid gray lines indicate Gaussian and biexponential fits to the data in (e) and (f), respectively. A band-pass filter was applied to the image in (a) to reduce artifacts from interference between the incident and reflected laser beam.

light microscopy. While the bright features show a tendency to be in close proximity of grain boundaries, they do not appear to conform to single grains. Indeed, the size of these features varies and they occur within the interior of individual perovskite grains. For ease of comparison, an overlay of the PL map onto the reflected light micrograph is provided in Figure S11 (Supporting Information) as a composite image. Curiously, excitation of the perovskite film from the glass-perovskite interface shows sharply defined grain boundaries exhibiting low intensity but highly uniform PL from the interior of the grains (Figure 5c). The strong subgranular variation in PL in these films is thus a feature unique to the top surface of the perovskite film and does not stem from structural features that extend throughout the bulk of the film. This is further confirmed by the lack of a correlation between areas of high luminescence and individual crystal domains in the fluorescence and polarized white-light transmission micrographs in Figure S12 (Supporting Information). A similar observation has recently been reported for the 3D perovskite FAPbI₃, where special subgrain boundaries with increased nonradiative recombination were found to exist in apparent single grains.^[36]

To better understand the nature of these variations, we selectively probed the PL at a representative bright and dark area in

the map of Figure 5d. The bright and dark areas are denoted as spot A (black) and spot B (red), respectively. The integrated PL spectra of both these areas are displayed in Figure 5e and show no apparent difference other than the expected difference in intensity. The time-resolved decay profiles of the PL in Figure 5f show a biexponential decay with a fast and slow decaying component $\tau_{\text{fast}} = 75$ ps (63%) and $\tau_{\text{slow}} = 363$ ps (37%) for the dark spot, which are both considerably prolonged for the bright spot for $\tau_{\text{fast}} = 92$ ps (66%) and $\tau_{\text{slow}} = 492$ ps (34%). Reduced PL intensity consequently coincides with a reduced PL lifetime, which indicates the presence of additional nonradiative decay channels due to trap states.

The spatial variation in PL intensities shows a strong dependence on the sample temperature. As can be seen in Figure 6a, the heterogeneity becomes more pronounced as the temperature increases (additional data given in Figure S13 in the Supporting Information). We probe the PL decay dynamics at both 10 and 293 K in the areas indicated in Figure 6b,c, in which the red circle indicates an area that is perceived as darkened at room temperature and the black circle denotes a bright area. We find that at 10 K the difference between the PL lifetime of the spots vanishes almost entirely and shows a small increase with respect to the PL lifetime of the bright spot

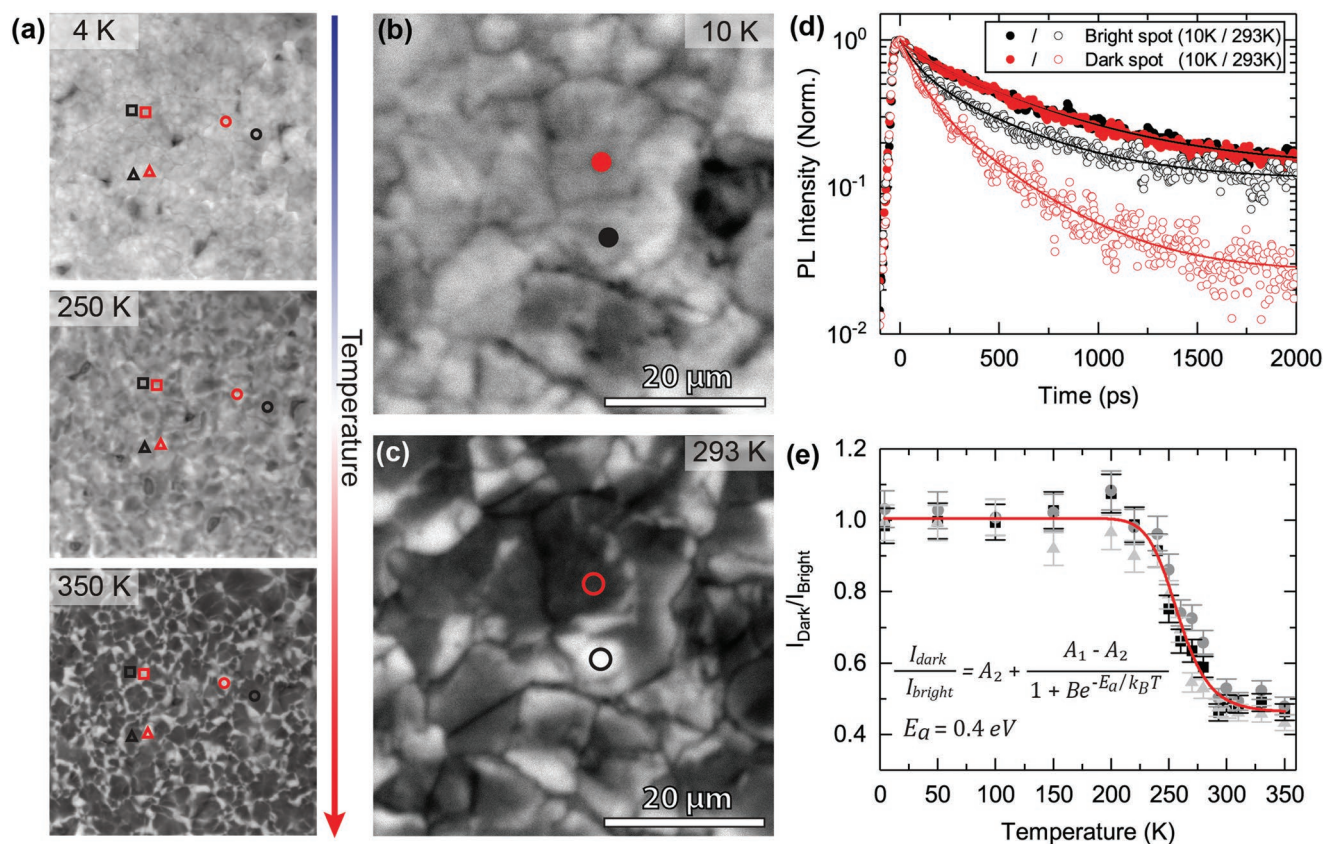


Figure 6. a) PL intensity map of the perovskite film at selected temperatures, demonstrating the temperature dependence of spatial variation in PLQY. Images are $50 \mu\text{m} \times 50 \mu\text{m}$. b,c) Close-up PL map of the (PEA)₂PbI₄ film at 10 and 293 K, respectively. d) TRPL traces obtained from both a bright (black) and dark (red) area at 10 K (filled symbols) and 293 K (open symbols) with their corresponding biexponential fits (solid lines). e) Plot of the ratio of the PL intensity at a dark spot (I_{dark}) and that of a bright spot (I_{bright}) as a function of temperature obtained from three independent combinations of a dark and bright spot (indicated by the different symbol shapes in A and E, where in A a black symbol denotes a bright area and red a dark area). The red line shows a modified Arrhenius fit to the data with an inflection point at 258 K and an activation energy of 0.4 eV.

at room temperature (Figure 6d). The trapping mechanism responsible for recombination in the darkened regions at room temperature is thus fully suppressed at cryogenic temperatures. Plotting the ratio of PL intensity $I_{\text{dark}}/I_{\text{bright}}$ of the dark and bright areas indicated by the symbols in Figure 6a over the full temperature range reveals a transition from the relatively homogeneous “bright state” at low temperatures to a highly heterogeneous “dark state” at high temperatures, as indicated in Figure 6e. This behavior can be described adequately by a modified Arrhenius equation (red line) with an inflection point around 260 K, corresponding to a large activation energy of 0.4 eV for this nonradiative recombination channel. This transition can also be clearly observed in the normalized histograms of the PL maps shown in Figure S14 (Supporting Information). While at low temperature the histogram appears to be closely matching a Gaussian distribution, indicating a single type of emitting species, a clear shoulder due to the bright features develops at higher PL intensity upon temperature increase.

At this point it should be noted that despite the homogeneous appearance of the film on a macroscopic scale, the size and density of these bright spots and grains on a microscopic scale does depend strongly on the area of the blade-coated film under investigation. Within a single film, one can find areas that show a large number of small bright features, whereas other areas have fewer but larger features. In some extreme cases, we observed circular features that can be as large as 200 micrometers in diameter. These features manifest themselves as areas of high PL intensity in CLSM and can also be readily observed in reflected light microscopy (Figure S15, Supporting Information). Considering the relatively fast crystallization of hybrid perovskites from solution and the large difference between the top and bottom surface of our films, it is reasonable to assume that the spatial distribution of trap states strongly depends on the crystallization process. It has in fact been recently reported that local depletion/enrichment of the precursor solution during crystallization has a very strong influence on the crystallization dynamics during the blade-coating of 3D perovskites, resulting in local differences in morphology and PL.^[37,38]

We therefore rationalize our findings in the context of local differences in the stoichiometry of the precursor solution during the film's crystallization: regions that are relatively enriched or depleted in either PbI_2 or PEAI will strongly impact the dynamics of the crystallization and therefore the local crystal quality. A local deficiency in one of the precursors is expected to lead to a large number of dangling bonds and associated trap states; creating areas of reduced luminescence in the film. In contrast, a local enrichment in PEAI or PbI_2 might effectively passivate such trap states and will be witnessed as a relatively bright area.

3. Conclusion

In summary, we have fabricated thin films of the Ruddlesden-Popper perovskite $(\text{PEA})_2\text{PbI}_4$ from precursor solutions of different stoichiometry using a scalable blade-coating technique. The stoichiometry of the precursor solution is found to have a pronounced influence on the crystallinity, morphology and

optical properties of the thin films. Even for films that are cast from a stoichiometric precursor solution, a large degree of heterogeneity in photoluminescence intensities was observed on a microscopic scale with local variations in PL occurring on a subgranular level. From low-temperature PL measurements, we were able to identify a nonradiative recombination channel with an activation energy of 0.4 eV that is responsible for the local reduction in PL intensity. This spatial variation likely arises from local fluctuations in the stoichiometry and a spatial distribution of surface trap states. By applying an excess of PEAI to the as-cast film, the photoluminescence intensity can be increased by as much as 85%, providing a simple way to reduce nonradiative recombination without affecting the morphology or crystallinity of the film. The findings of this work thus illustrate the potential of blade-coating as a means to deposit high-quality 2D perovskite films for optoelectronic applications and underline the crucial role stoichiometry and crystallization dynamics play in the microscopic properties of such films.

4. Experimental Section

Film Fabrication: Thin films were cast on glass substrates, which were ultrasonically cleaned sequentially in detergent solution, deionized water, acetone, and isopropanol. After drying in an oven at 140 °C for at least 10 min, the substrates were treated with ultraviolet ozone for 20 min and immediately transferred into a nitrogen-filled glovebox for film deposition.

The 2D $(\text{PEA})_2\text{PbI}_4$ perovskite precursor solution was prepared by dissolving PEAI (98.0% TCI) and PbI_2 (99.99% TCI) at a molar ratio as given in the main text in a mixed solvent of DMF and DMSO (volume ratio 4:1) to form a solution of 0.5 M in concentration. The solutions were stirred for at least 3 h at room temperature before deposition. To blade-coat the 2D films, the glass substrates were preheated and held at a temperature of 80 °C. The precursor solution was dropped onto the substrate and swiped linearly by a metal blade at a speed of 10 mm s⁻¹. The gap between the glass substrate and the blade was fixed at 400 μm. The spin coated films were fabricated using a two-step spin coating process with antisolvent treatment. The spin coating process uses 1000 rpm for 10 s followed by 4000 rpm for 30 s. 10 s prior to the end of the spin coating cycle the antisolvent (chlorobenzene) was added to the film. In both cases the films were immediately annealed at 100 °C for 10 min.

Absorption Measurements: Absorption measurements were performed using a UV–vis–NIR spectrophotometer (Shimadzu UV-3600).

Photoluminescence Spectroscopy: For the PL measurements, the samples were excited by the second harmonic (400 nm) of a mode-locked Ti:sapphire laser (Mira900, Coherent). The beam was spatially confined by passing through an adjustable iris. The beam power was adjusted by the use of adjustable neutral density filters. The PL of the sample was collected and focused onto a monochromator with 50 lines mm⁻¹ and the dispersed spectrum was then imaged by a Hamamatsu image CCD. For time-resolved measurements, a Hamamatsu streak camera operating in synchroscan or single-sweep mode was used to disperse the photoluminescence signal in time with the appropriate temporal resolution.

Confocal Laser Scanning Microscopy: A Nikon C1 confocal microscope system was used to capture CLSM images, fluorescence and transmission micrographs. For this, either a 40× ELWD objective or an oil-immersion 100× objective was used. For CLSM, samples were excited by a 488 nm continuous wave laser, the principal beam of an 800 nm pulsed laser or the second harmonic of this laser. The photoluminescence map was captured using photomultiplier tubes operating in the spectral region 485–545 nm, or by recording the output

of the optical fiber with the system described under photoluminescence spectroscopy.

Reflected Light Microscopy: Reflected-light micrographs were captured using an Olympus BX51M microscope equipped with 5 \times , 10 \times , and 50 \times objectives and an Olympus ColorView Camera.

X-Ray Diffraction: X-ray diffraction was performed under ambient conditions. The X-ray data were collected using a Bruker D8 Advanced diffractometer in Bragg–Brentano geometry and operating with a Cu K α radiation source ($\lambda = 1.54 \text{ \AA}$) and Lynxeye detector.

Atomic Force Microscopy: The atomic force microscopy (AFM) images were taken using a Bruker NanoScope V instrument in the ScanAsyst mode.

Scanning Electron Microscopy: The scanning electron microscopy (SEM) images were obtained using an FEI Nova Nano SEM 650 instrument with an accelerating voltage of 10 kV and a low-vacuum GAD detector.

Supporting Information

Supporting Information is available from the Wiley Online Library or from the author.

Acknowledgements

The authors express their gratitude to A. F. Kamp and T. Zaharia for their technical support and G. R. Blake for valuable discussions. J. C. Alonso Huitrón is gratefully acknowledged for the calculation of the CIE coordinates of the photoluminescence, and the authors also thank A. A. Mura and V. Sarritzu for measurements of the PLQY. S.K. acknowledges the Deutsche Forschungsgemeinschaft (DFG) for a postdoctoral research fellowship (Grant No. 408012143). This work is part of the research program of the Foundation for Fundamental Research on Matter (FOM), which is part of the Netherlands Organization for Scientific Research (NWO). This is a publication of the FOM-focus Group “Next Generation Organic Photovoltaics,” participating in the Dutch Institute for Fundamental Energy Research (DIFFER).

Conflict of Interest

The authors declare no conflict of interest.

Keywords

2D perovskites, passivation, photoluminescence, trap states

Received: September 10, 2019

Revised: October 25, 2019

Published online:

- [1] S. D. Stranks, G. E. Eperon, G. Grancini, C. Menelaou, M. J. P. Alcocer, T. Leijtens, L. M. Herz, A. Petrozza, H. J. Snaith, *Science* **2013**, 342, 341.
- [2] Y. Bi, E. M. Hutter, Y. Fang, Q. Dong, J. Huang, T. J. Savenije, *J. Phys. Chem. Lett.* **2016**, 7, 923.
- [3] National Renewable Energy Laboratory, NREL Efficiency Chart 2019, <https://www.nrel.gov/pv/cell-efficiency.html> (accessed: August 2019).
- [4] Z.-K. Tan, R. S. Moghaddam, M. L. Lai, P. Docampo, R. Higler, F. Deschler, M. Price, A. Sadhanala, L. M. Pazos, D. Credgington, F. Hanusch, T. Bein, H. J. Snaith, R. H. Friend, *Nat. Nanotechnol.* **2014**, 9, 687.
- [5] L. Zhang, X. Yang, Q. Jiang, P. Wang, Z. Yin, X. Zhang, H. Tan, Y. M. Yang, M. Wei, B. R. Sutherland, E. H. Sargent, J. You, *Nat. Commun.* **2017**, 8, 15640.
- [6] L. N. Quan, F. P. García de Arquer, R. P. Sabatini, E. H. Sargent, *Adv. Mater.* **2018**, 30, 1801996.
- [7] H. Wei, Y. Fang, P. Mulligan, W. Chuirazzi, H. H. Fang, C. Wang, B. R. Ecker, Y. Gao, M. A. Loi, L. Cao, J. Huang, *Nat. Photonics* **2016**, 10, 333.
- [8] H.-H. Fang, S. Adjokatse, H. Wei, J. Yang, G. R. Blake, J. Huang, J. Even, M. A. Loi, *Sci. Adv.* **2016**, 2, e1600534.
- [9] Q. Chen, N. De Marco, Y. Yang, T. Bin Song, C. C. Chen, H. Zhao, Z. Hong, H. Zhou, Y. Yang, *Nano Today* **2015**, 10, 355.
- [10] J. Sun, J. Wu, X. Tong, F. Lin, Y. Wang, Z. M. Wang, *Adv. Sci.* **2018**, 5, 1700780.
- [11] H. Lin, C. Zhou, Y. Tian, T. Siegrist, B. Ma, *ACS Energy Lett.* **2018**, 3, 54.
- [12] Z. Cheng, J. Lin, J. Walter, H. Dreyse, Z. Sui, J. Liu, J. Lin, A. Qin, W. Yuan, H. Chen, M. Wang, B. Tang, F. Milia, G. Chapuis, *CrystEngComm* **2010**, 12, 2646.
- [13] L. Pedesseau, D. Saporì, B. Traore, R. Robles, H.-H. Fang, M. A. Loi, H. Tsai, W. Nie, J.-C. Blancon, A. Neukirch, S. Tretiak, A. D. Mohite, C. Katan, J. Even, M. L. Kepenekian, *ACS Nano* **2016**, 10, 9776.
- [14] X. Hong, T. Ishihara, A. V. Nurmikko, *Phys. Rev. B* **1992**, 45, 6961.
- [15] J. C. Blancon, A. V. Stier, H. Tsai, W. Nie, C. C. Stoumpos, B. Traoré, L. Pedesseau, M. Kepenekian, F. Katsutani, G. T. Noe, J. Kono, S. Tretiak, S. A. Crooker, C. Katan, M. G. Kanatzidis, J. J. Crochet, J. Even, A. D. Mohite, *Nat. Commun.* **2018**, 9, 2254.
- [16] R. K. Misra, B. El Cohen, L. Iagher, L. Etgar, *ChemSusChem* **2017**, 10, 3712.
- [17] J. Xing, Y. Zhao, M. Askerka, L. N. Quan, X. Gong, W. Zhao, J. Zhao, H. Tan, G. Long, L. Gao, Z. Yang, O. Voznyy, J. Tang, Z. H. Lu, Q. Xiong, E. H. Sargent, *Nat. Commun.* **2018**, 9, 3541.
- [18] X. Yang, X. Zhang, J. Deng, Z. Chu, Q. Jiang, J. Meng, P. Wang, L. Zhang, Z. Yin, J. You, *Nat. Commun.* **2018**, 9, 570.
- [19] Y. Tian, C. Zhou, M. Worku, X. Wang, Y. Ling, H. Gao, Y. Zhou, Y. Miao, J. Guan, B. Ma, *Adv. Mater.* **2018**, 30, 1707093.
- [20] X. Zhao, J. D. A. Ng, R. H. Friend, Z. K. Tan, *ACS Photonics* **2018**, 5, 3866.
- [21] S. Adjokatse, H. H. Fang, H. Duim, M. A. Loi, *Nanoscale* **2019**, 11, 5989.
- [22] T. Zhao, H. Liu, M. E. Ziffer, A. Rajagopal, L. Zuo, D. S. Ginger, X. Li, A. K. Y. Jen, *ACS Energy Lett.* **2018**, 3, 1662.
- [23] Y. Zhang, F. Li, K. Jiang, J.-H. Huang, H. Wang, H. Fan, P. Wang, C.-M. Liu, L.-P. Zhang, Y. Song, *J. Mater. Chem. A* **2018**, 6, 17867.
- [24] E. M. Tennyson, T. A. S. Doherty, S. D. Stranks, *Nat. Rev. Mater.* **2019**, 4, 573.
- [25] B. J. Foley, S. Cuthriell, S. Yazdi, A. Z. Chen, S. M. Guthrie, X. Deng, G. Giri, S. H. Lee, K. Xiao, B. Doughty, Y. Z. Ma, J. J. Choi, *Nano Lett.* **2018**, 18, 6271.
- [26] W. Liu, J. Xing, J. Zhao, X. Wen, K. Wang, P. Lu, Q. Xiong, *Adv. Opt. Mater.* **2017**, 5, 1601045.
- [27] M. Yuan, L. N. Quan, R. Comin, G. Walters, R. Sabatini, O. Voznyy, S. Hoogland, Y. Zhao, E. M. Beauregard, P. Kanjanaboos, Z. Lu, D. H. Kim, E. H. Sargent, *Nat. Nanotechnol.* **2016**, 11, 872.
- [28] H.-D. Lee, H. Kim, H. Cho, W. Cha, Y. Hong, Y.-H. Kim, A. Sadhanala, V. Venugopalan, J. S. Kim, J. W. Choi, C.-L. Lee, D. Kim, H. Yang, R. H. Friend, T.-W. Lee, *Adv. Funct. Mater.* **2019**, 29, 1901225.
- [29] H. Duim, H.-H. Fang, S. Adjokatse, G. H. ten Brink, M. A. L. Marques, B. J. Kooi, G. R. Blake, S. Botti, M. A. Loi, *Appl. Phys. Rev.* **2019**, 6, 031401.

- [30] M. G. La-Placa, G. Longo, A. Babaei, L. Martínez-Sarti, M. Sessolo, H. J. Bolink, *Chem. Commun.* **2017**, 53, 8707.
- [31] R. Quintero-Bermudez, A. H. Proppe, A. Mahata, P. Todorovic, S. O. Kelley, F. De Angelis, E. H. Sargent, *J. Am. Chem. Soc.* **2019**, 141, 13459.
- [32] S. Shao, J. Liu, G. Portale, H. H. Fang, G. R. Blake, G. H. ten Brink, L. J. A. Koster, M. A. Loi, *Adv. Energy Mater.* **2018**, 8, 1702019.
- [33] S. Adjokatse, J. Kardula, H. H. Fang, S. Shao, G. H. ten Brink, M. A. Loi, *Adv. Mater. Interfaces* **2019**, 6, 1801667.
- [34] H. H. Fang, J. Yang, S. Tao, S. Adjokatse, M. E. Kamminga, J. Ye, G. R. Blake, J. Even, M. A. Loi, *Adv. Funct. Mater.* **2018**, 28, 1800305.
- [35] M. D. Smith, H. I. Karunadasa, *Acc. Chem. Res.* **2018**, 51, 619.
- [36] W. Li, S. K. Yadavalli, D. Lizarazo-Ferro, M. Chen, Y. Zhou, N. P. Padture, R. Zia, *ACS Energy Lett.* **2018**, 3, 2669.
- [37] Z. Bi, X. Rodríguez-Martínez, C. Aranda, E. Pascual San José, A. R. Goni, M. Campoy-Quiles, X. Xu, A. Guerrero, *J. Mater. Chem. A* **2018**, 6, 19085.
- [38] Z. Yang, C. C. Chueh, F. Zuo, J. H. Kim, P. W. Liang, A. K. Y. Jen, *Adv. Energy Mater.* **2015**, 5, 1500328.